INSTITUTE OF PHYSICS PUBLISHING JOURNAL OF RADIOLOGICAL PROTECTION

J. Radiol. Prot. **26** (2006) 277–286 doi:10.1088/0952-4746/26/3/002

Radiological characterisation of photon radiation from ultra-high-intensity laser–plasma and nuclear interactions

R J Clarke[1,2], D Neely[1], R D Edwards[3], P N M Wright[1], K W D Ledingham[2,3], R Heathcote[1], P McKenna[1,2], C N Danson[1], P A Brummitt[1], J L Collier[1], P E Hatton[1], S J Hawkes[1], C Hernandez-Gomez[1], P Holligan[1], M H R Hutchinson[1], A K Kidd[1], W J Lester[1], D R Neville[1], P A Norreys[1], D A Pepler[1], T B Winstone[1], R W W Wyatt[1] and B E Wyborn[1]

[1] CCLRC Rutherford Appleton Laboratory, Chilton, Didcot OX11 0QX, UK
[2] SUPA, Department of Physics, University of Strathclyde, Glasgow G4 0NG, UK
[3] AWE plc, Aldermaston, Reading RG7 4PR, UK

E-mail: r.j.clarke@rl.ac.uk

Received 5 January 2006, accepted for publication 18 May 2006
Published 21 August 2006
Online at stacks.iop.org/JRP/26/277

Abstract

With the increasing number of multi-terawatt (10^{12} W) and petawatt (10^{15} W) laser interaction facilities being built, the need for a detailed understanding of the potential radiological hazards is required and their impact on personnel is of major concern. Experiments at a number of facilities are being undertaken to achieve this aim. This paper describes the recent work completed on the Vulcan petawatt laser system at the CCLRC Rutherford Appleton Laboratory, where photon doses of up to 43 mSv at 1 m per shot have been measured during commissioning studies. It also overviews the shielding in place on the facility in order to comply with the Ionising Radiation Regulations 1999 (IRR99), maintaining a dose to personnel of less than 1 mSv yr^{-1} and as low as reasonably practicable (ALARP).

(Some figures in this article are in colour only in the electronic version)

1. Introduction

At laser interaction intensities of greater than 10^{18} W cm^{-2}, a significant part of the laser energy is converted into the generation of high-energy electrons, leading to the emission of high-energy Bremsstrahlung. Secondary effects through target charging and nuclear reactions lead to the acceleration of protons, ions and neutrons, dominated by (p, n) and (γ, n) reactions; the detailed production of these is discussed elsewhere [1–3]. The emission of high-energy

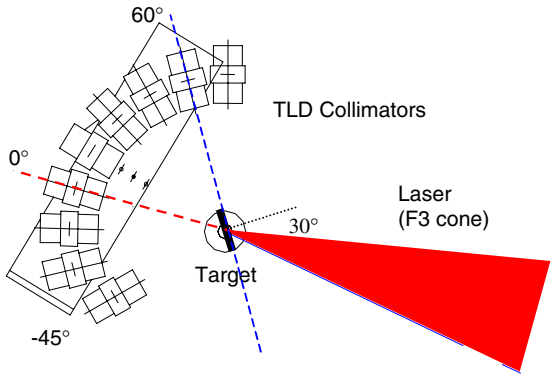

Figure 1. Thermoluminesense detector (TLD) positions relative to the target and laser axis.

Bremsstrahlung is particularly significant due to its high transmission through most materials and its effect on the human body. The protection against this type of radiation is now a major part of the design for any high-power laser interaction facility in order to comply with IRR99 [4]. Recent experiments have shown that protection against photon emission dominates the shielding requirements when compared to that required for protection against neutron radiation. Recently published data [5] have identified the strong need for radiological shielding on operational facilities with intensities in the order of 10^{19} W cm^{-2}. Since then, a number of laser facilities with petawatt capabilities (10^{15} W) have been, or are in the process of being, constructed across the world and the motivation of this paper is to characterise for the first time the much larger radiological implications of such facilities.

2. Laser system

The Vulcan laser system [6] utilises the technique of chirped pulse amplification (CPA) [7] to generate both a 100 TW beamline and a 1 PW beamline. The 100 TW facility operates at $\sim$1 ps, and up to 90 J on target, regularly achieving mid 10^{19} W cm^{-2} using an F3 focusing optic. The petawatt facility, during the period of commissioning, operated at $\sim$1 ps, with on-target energies up to 250 J. The focusing optic was an F3 off-axis parabolic mirror producing a 5 μm full width half maximum (FWHM) focal spot. The percentage of laser energy contained within the spot is estimated to be 30%. The laser energy was varied to produce intensities between 5×10^{19} W cm^{-2} and 4×10^{20} W cm^{-2}. The target angle for all experiments was $\sim$30° (see figure 1).

3. Radiation shielding

The 100 TW facility uses removable lead shielding to provide radiological protection for the facility staff and user groups. These have been shown to reduce the radiation level below that detectable by commercial Landauer personal dosimeters with typical resolution of 0.01 mSv. The petawatt facility, however, uses permanent in-built shielding as part of the facility design. This was considered necessary not only due to the high predicted doses for the facility, but also as the facility is surrounded by occupied buildings. The primary photon shielding in place on the Vulcan petawatt facility consists of 15 cm thick localised lead shielding surrounding the laser interaction chamber. In addition, the facility walls are 60 cm thick concrete, providing additional secondary shielding and protection against scattered radiation. The primary shielding around the interaction chamber can be seen in figure 2. The

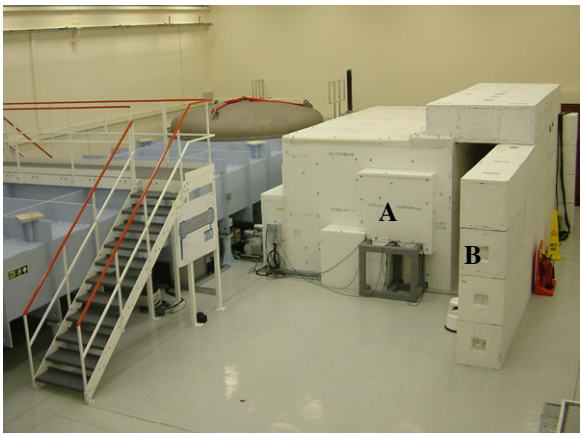

Figure 2. Petawatt target chamber with primary photon and neutron shielding.

concrete, in addition to 10 cm of localised high-density polyethylene around the chamber, also provides neutron shielding for the facility. Back-shielding is provided for diagnostic ports (figure 2(A)) and the chamber entrance (figure 2(B)) for both photon and neutron radiation, equivalent to the primary shielding surrounding the chamber. In total, the facility shielding has an attenuation of $\sim 10^5$ for photons at its peak transmission of $\sim$4 MeV. With a minimum distance to an occupied area of 5 m, this gives the facility an overall attenuation of $\sim 2 \times 10^6$ from measurements normalised to 1 m.

4. Radiation measurements

The experimental goals were based on the requirement to commission the radiological shielding of the petawatt facility. The main aim was to assess the photon dose produced from high atomic number (Z) target materials at the maximum on-target intensity achievable at the time of commissioning. In order to ensure the maximum safety for personnel, shots began at intensities of mid 10^{19} W cm^{-2} where 100 TW data already exist. The intensity was then varied by changing the laser energy whilst maintaining a fixed pulse length. Different target thickness and target Z were also used to monitor the effects. Work began on low-Z targets as the high-energy components of the radiation were expected to increase with target Z.

All radiological data were collected on single shots using TLD700 thermoluminescence detector (TLD) powder, calibrated to an NPL standard and cross-referenced to commercial personal dosimeters during the experiment. The TLD700 dosimeters were selected as their spectral response reflects that of human tissue. Unlike the commonly used TLD100 dosimeter, the TLD700 also has a very low sensitivity to neutrons. The TLDs were used in a filtered tungsten collimator [8] as shown in figure 3(a) using tungsten filters in order to collect spectral information on the measured radiation. The incident spectrum for each TLD, calculated from mass attenuation coefficient data [9], can be seen in figure 3(b).

The TLDs were positioned radially on the horizontal plane at $\sim 15°$ intervals from $-45°$ to 80° to the laser axis, as shown in figure 1. This enabled the angular distribution of the primary radiological direction to be investigated. Previous data have shown that the directionality of the emitted photons is dependent upon the different absorption mechanisms present [8, 10, 11]. All measurements were performed inside the laser interaction chamber in order to characterise the emitted radiation with minimum shielding effects.

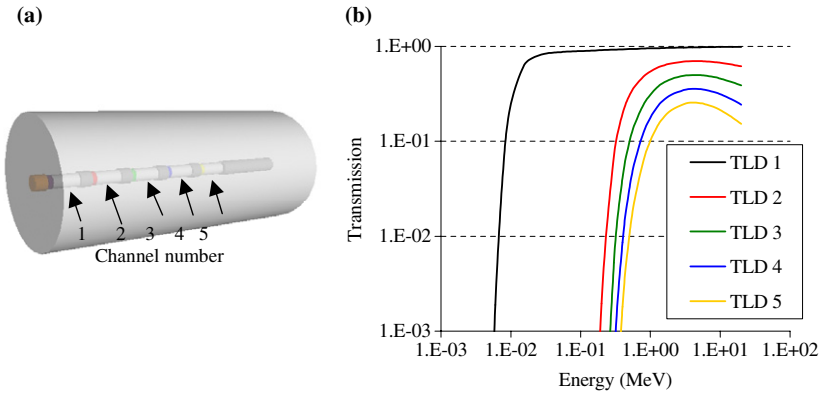

Figure 3. (a) TLD collimator, and (b) spectral cut-off for each TLD used to measure the spectral components.

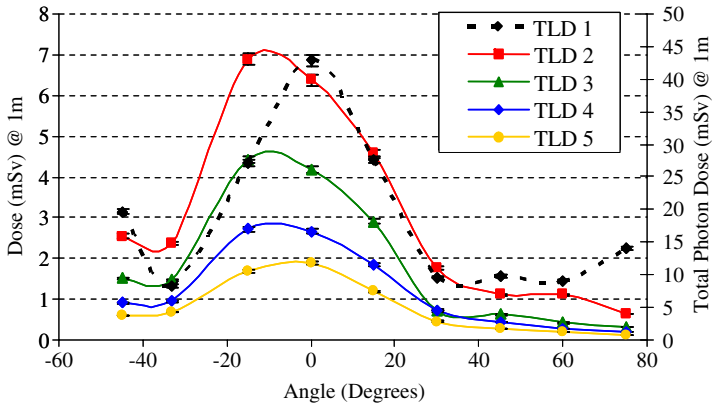

Figure 4. TLD summary for 1 mm gold target. Angles are shown relative to the laser forward direction. $I \sim 4 \times 10^{20}$ W cm^{-2}, $E \sim 230$ J. Total photon dose is shown as a dotted line corresponding to the right axis.

5. Results

The data collected from the TLDs indicate a peak photon emission in the forward laser direction. This peak emission extends over a 40° cone angle [11] and can be seen in figure 4. This figure shows the angular variation of dose for each of the filtered TLDs. The right axis applies to the total photon dose (TLD 1—dotted line) and the left axis to the dose for the higher energy filtered TLDs (TLD 2 to TLD 5). The peak photon dose observed during the experiment was 43 mSv at 1 m. The on-target intensity was $\sim 4 \times 10^{20}$ W cm^{-2}, with ~230 J on a 1 mm thick gold target. The peak is observed along the laser forward direction, but has some asymmetry towards the target normal (−30°). Previous observations [10, 11] have shown that the direction of the photon peak can vary with a change in plasma scale length, typically caused through amplified spontaneous emission (ASE) or pre-pulses on the laser. This can easily explain a slight asymmetry in this direction.

In order to compare the generated dose at different laser energies, the unit of dose per Joule at 1 m is used. Figure 5 shows the collated data for the maximum dose measured on each shot.

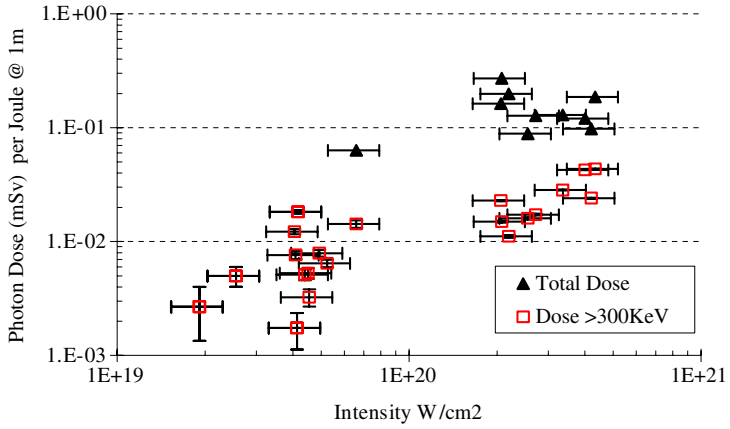

Figure 5. Total dose and dose >300 keV J^{-1} of laser energy as a function of laser intensity for 1 and 3 mm gold targets.

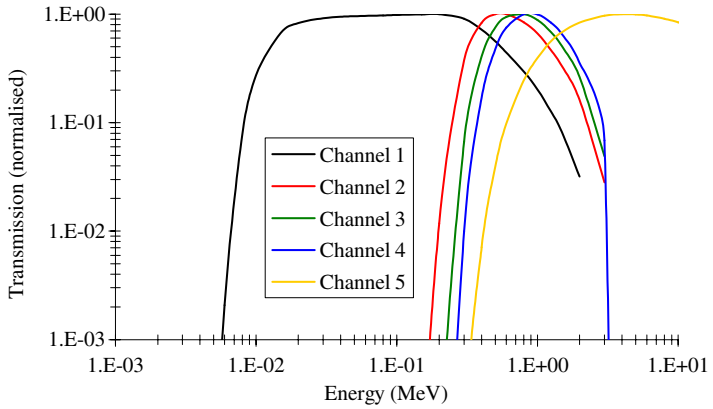

Figure 6. Spectral response bands generated by subtraction of TLD data.

Both the total dose and the dose above 300 keV (TLD 2), are plotted as a function of dose per Joule of laser energy against on-target intensity.

The dose above 300 keV is significant as it is more representative of that transmitted through the interaction chamber wall. The filtering of each TLD allows a comparison of the spectral content of the photon radiation emitted from different target types up to ∼4 MeV. By subtracting the doses from two subsequent TLDs in the same collimator, the dose contained within a small spectral band can be inferred. These spectral bands are shown in figure 6 and the spectral data for the various target types can be seen in figures 7 and 8. Figure 7 illustrates the differences in the spectral components as the target Z increases. It can be seen that as the target Z increases, the higher spectral component also increases, by a factor of 6.5 between the CH (plastic) targets and the Au targets at ∼4 MeV.

Figure 8 highlights that 3 mm Au targets do not significantly increase the high-energy components, and only serve to reduce the low-energy components due to the self-attenuation effects of the target itself. The thick, high-Z targets attenuate photons below the 300 keV level, compared to the thinner high-Z and low-Z targets.

A side peak was commonly observed between 40° and 60° from the laser forward axis, corresponding to the target plane. This peak was also observed above the target, where a dose greater than the isotropic emission was measured. Examples of these shots can be seen in figures 9(a) and (b). Slight angular changes in the direction of the side peak can be explained thorough variations in the target angle between shots.

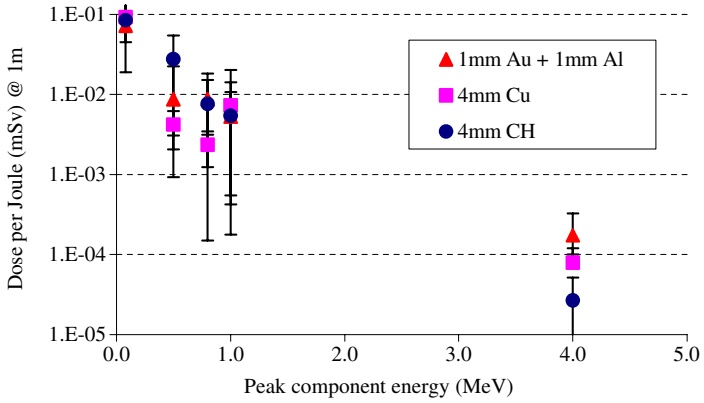

Figure 7. Spectral components from different target type and thickness. Data are plotted at the peak energy of the spectral band.

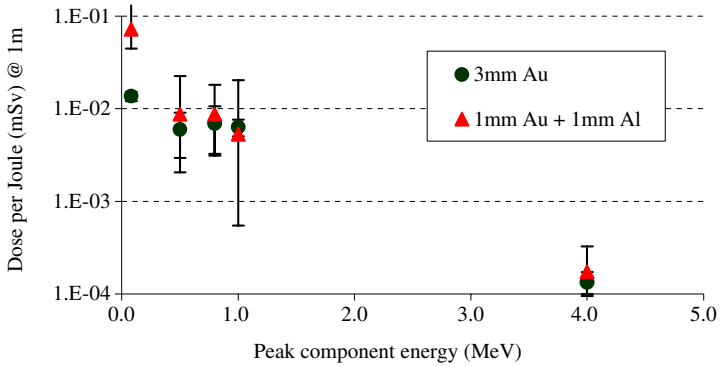

Figure 8. Spectral components from gold targets of different thickness. Data are plotted at the peak energy of the spectral band.

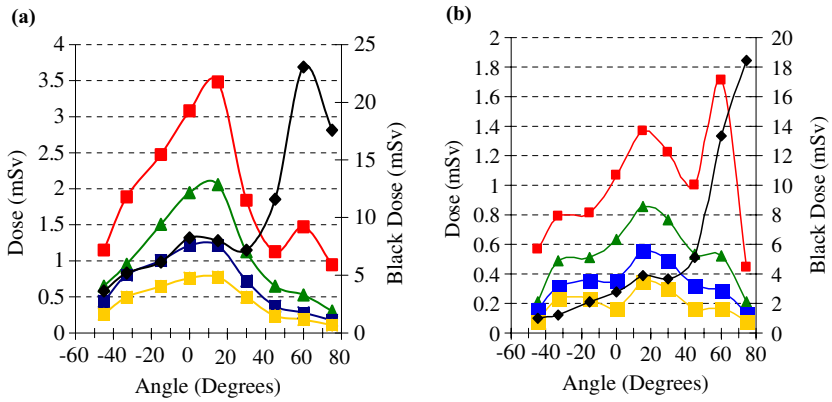

Figure 9. Raw data for 178 J (a) and 144 J (b) shots on 3 mm gold targets. Angles are shown relative to the laser forward direction. On-target intensity was $\sim 2 \times 10^{20}$ W cm^{-2}.

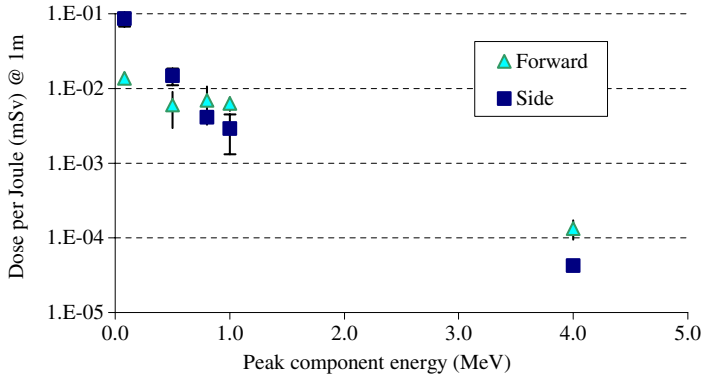

Figure 10. A comparison of the spectral components of the forward and side peaks for 3 mm gold targets.

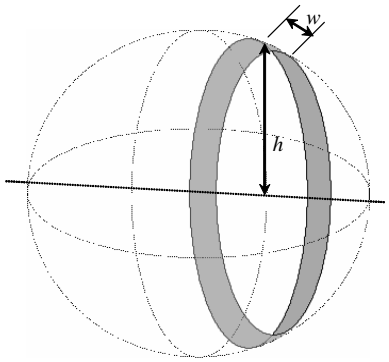

Figure 11. Segmented sphere used to analyse the forward energy components.

Shots taken on the 3 mm gold targets produced a side peak with doses high enough for a spectral measurement to be made. A comparison between the main forward peak and this side peak is shown in figure 10. From these data, it can be seen that there is a factor of ∼5 difference between the forward and side peaks in the low-energy region. The difference can be explained by self-attenuation in the target itself, as the targets are thinner in the direction of the target plane compared to the forward direction for the 3 mm gold targets, as the targets were also 3 mm in diameter. This highlights the requirement for shielding outside of the forward laser direction where the peak radiation emission is usually observed.

Figure 10 confirms that the high-energy electrons, which generate the higher energy photon components, are directed along the laser forward direction. Although the peak dose is in the forward laser direction, there is a significant component that is emitted into 4π. This is evident in figures 4 and 9, where the isotropic dose remains above 0.5 mSv at 1 m. Assuming a sphere of radius 1 m, the surface area covered by the forward peak is very low compared to the surface area covered by the isotropic dose. An analysis accounting for the ratio of emitted radiation over a sphere gives a quantitative value of the percentage of emitted radiation in the forward cone.

Previous measurements [10, 11] show symmetry between the emitted radiation in the horizontal and vertical planes for the forward peak. For the following analysis, it was assumed that this symmetry extends over the sphere. The collected data enable a calculation of the dose contained within a segment of the 1 m sphere around the target, as shown in figure 11, using the equation for the area of each segment

$$\text{Area of segment } (S) = 2\pi hw$$

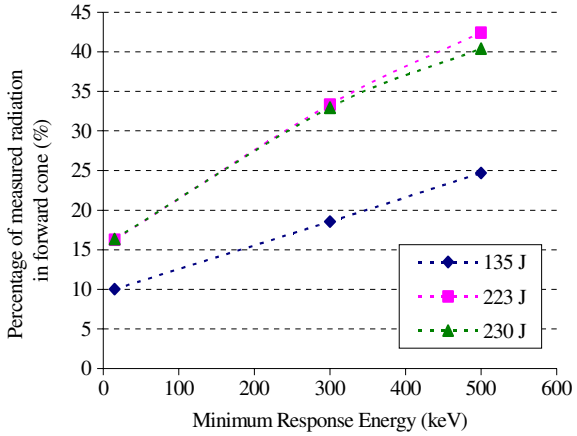

Figure 12. Percentage of the measured radiation within the forward peak. Data are plotted against the minimum response energy of the TLDs. Peak total doses measured are 12 mSv (135 J), 22 mSv (223 J) and 43 mSv (230 J).

and summing the dose per segment (D) over all segments (S) of the sphere using the equation

$$\text{Integrated dose} = \sum_n S_n D_n.$$

The emitted radiation per unit area can be calculated and a determination of the radiation components within the forward peak is made. This calculation reduces the three-dimensional emission from the target to a two-dimensional analytical technique.

For this calculation it is also assumed that no peak exists from the front of the target (towards the incident laser beam). The data presented in figure 12, for three different shots, are plotted against the minimum energy response of the TLDs, as the incident spectra on the TLDs (figure 3(b)) is used for this evaluation rather than the spectral bands (figure 6). This is for simplification purposes only. It should be noted that, using this technique, the TLDs plotted at lower energies actually see all photons above their minimum response energy.

The forward 40° cone contains less than 20% of the total emitted dose and shows an increase as the laser energy (and hence intensity) is increased. Therefore, over 80% of the low-energy photons are emitted isotropically. It is also apparent that a maximum of 40% of the higher energy components are directed into this cone. This also shows an increase as the laser energy is increased.

For photon energies above a few MeV, it becomes difficult to measure the radiation using TLDs. This is due to (a) the sensitivity of the detector after the filtration required to block the lower energies and (b) the turnover point apparent in the mass attenuation curves (see figure 3(b)). Because of this difficulty, the favoured method to measure the high-energy components is via scintillation detectors [10] or by (γ, n), (γ, 2n), etc and (γ, γ) reactions in materials producing secondary radioisotopes. Recent experiments have shown (γ, n) and (γ, 3n) reactions [12] in thick ($\sim$3 mm) gold targets taken on the Vulcan petawatt laser under similar pulse conditions. These results show 6.7×10^8 and 2.5×10^6 generated nuclei of the isotopes ^{196}Au and ^{194}Au respectively from the (γ, n) and (γ, 3n) reactions.

For high-energy (>10 MeV) photons, it can be assumed that a minimal loss of γ photons takes place within the target during the reactions, hence the equation

$$R = N\sigma$$

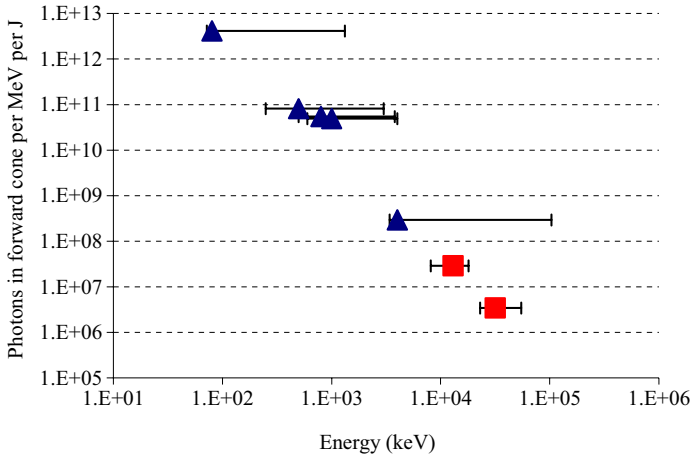

Figure 13. Photon numbers for the forward 40° cone based on TLD measurements (blue triangles) and induced activity from (γ, n) and (γ, 3n) reactions in the gold target (red squares). $I \sim 4 \times 10^{20}$ W cm^{-2}.

can be used to calculate the number of generated reactions per cm (R). N is the number of atoms per unit volume and σ is the cross-section in cm^2. An approximation fit to the cross-section data is used to determine the number of reactions per cm, and using the thickness of the target the number of photons required to generate the measured number nuclei of each isotope is made. This approximation is limited in accuracy by (a) the fit to the cross-section made in the calculations and (b) the assumption that the majority of electrons are converted to γ-rays at the front of the target and hence travel through the total target thickness.

The TLD measurements can be converted to photon numbers using known photon to flux data to derive a photon flux from the target interaction. As the data obtained from the (γ, n) and (γ, 3n) reactions include reactions over a larger solid angle than the raw TLD data, the TLD data used also need to reflect the same angle. Since the (γ, n) and (γ, 3n) reactions require photons above 10 MeV, and the high-energy photons fall mostly within the forward 40° cone, the TLD data can be restricted to the forward going 40° cone. This provides a representation of the total forward photon flux and is shown in figure 13. The energy error bars are equivalent to the bandwidth of each TLD channel (figure 6) or, for the (γ, n) and (γ, 3n) activation measurements, the full width half maximum (FWHM) of the cross-section.

6. Conclusion

The photon emission from a single shot on the Vulcan petawatt laser system has produced a peak photon dose of 43 mSv at 1 m with ~250 J on target, and appears to scale with both laser intensity and laser energy. These data correspond well to data from other facilities with differing laser parameters [5, 13–16] as well as simulated data [17].

The total measured dose has been observed to be relatively independent of target material due to the dominance of low-energy photons (<1 MeV), though a relationship with target material and thickness has been observed at photon energies above 300 keV. It has been shown that the peak dose is directed into the forward laser direction rather than into the forward target normal direction as has been previously published [8, 10, 11]. This can be explained by a difference in pre-pulse conditions [10, 11] or by the increase of the laser intensity which

changes the electron acceleration processes. The percentage of dose contained within the forward cone increases with the energy of the emitted radiation, but the total dose in the forward cone is less than 20% of the total emitted radiation from the target.

When operating at a full petawatt, the facility is expected to deliver an on-target intensity of $\sim 1 \times 10^{21}$ W cm^{-2}. At this intensity, the expected photon dose per shot will be ~ 0.6 mSv J^{-1} at 1 m. With approximately 300 shots yr^{-1} and an on-target energy of 400 J, the laser–target interaction will produce ~ 70 Sv yr^{-1} at 1 m. As the facility shielding provides a minimum attenuation of $\sim 2 \times 10^6$ (at ~ 4 MeV), the resultant dose expected to staff and visiting scientists will be less than 0.1 mSv yr^{-1}. This level falls well within the Ionising Radiation Regulations 1999 (IRR99). In practice, as the maximum shielding transmission is at ~ 4 MeV yet the peak photon emission is less than 1 MeV, the facility has an even greater safety factor. This allows for future upgrades to take place with minimal modifications to the facility shielding.

Acknowledgments

We would like to thank all those involved in the experimental programmes leading to the collection of the presented data. We would also like to thank the personnel from other large laser facilities across Europe and the United States for providing information with which to compare the collected data.

References

[1] Amiranoff F 2001 Fast electron production in ultra-short high-intensity laser–plasma interaction and its consequences *Meas. Sci. Technol.* **12** 1795–800
[2] Ledingham K W D, McKenna P and Singhal R P 2003 Applications for nuclear phenomena generated by ultra-intense lasers *Science* **300** 1107
[3] McKenna P *et al* 2003 Demonstration of fusion-evaporation and direct-interaction nuclear reactions using high-intensity laser–plasma-accelerated ion beams *Phys. Rev. Lett.* **91** 075006
[4] *Ionising Radiations Regulations* 1999 (London: HSE Books) (ISBN 0-7176-1746-7)
[5] Borne F, Delacroix D, Gelé J M, Massé D and Amiranoff A 2002 Radiation protection for an ultra-high intensity laser *Radiat. Prot. Dosim.* **102** 61
[6] Danson C N *et al* 2004 Vulcan petawatt—an ultra-high intensity interaction facility *IAEA J. Nucl. Fusion* **44** S239–46
[7] Strickland D and Mourou G 1985 Compression of amplified chirped optical pulses *Opt. Commun.* **56** 219
[8] Edwards R D *et al* 2002 Characterization of a gamma-ray source based on a laser–plasma accelerator with applications to radiography *Appl. Phys. Lett.* **80** 2129
[9] Hubbell J H and Seltzer S M 2004 *Tables of X-ray Mass Attenuation Coefficients and Mass Energy-Absorption Coefficients (version 1.4)* (Gaithersburg, MD: National Institute of Standards and Technology) (Online) available: http://physics.nist.gov/xaamdi
[10] Norreys P A *et al* 1999 Observation of a highly directional γ-ray beam from ultrashort, ultraintense laser pulse interactions with solids *Phys. Plasmas* **6** 2150
[11] Santala M I K *et al* 2000 Effect of the plasma density scale length on the direction of fast electrons in relativistic laser–solid Interactions *Phys. Rev. Lett.* **84** 1459
[12] Ledingham K W D *et al* 2003 Laser-driven photo-transmutation of ^{129}I—a long-lived nuclear waste product *J. Phys. D: Appl. Phys.* **36** L79–82
[13] Singh M 1999 private communication (Nova Laser, LLNL)
[14] Valentin C 2002 private communication (Salle Jaune Laser, Ecole Polytechnique)
[15] Edwards R D 2006 private communication (Helen Laser (upgrade commissioning results) AWE)
[16] Hatchett S P *et al* 2000 Electron, photon, and ion beams from the relativistic interaction of petawatt pulses with solid targets *Phys. Plasmas* **7** 2076
[17] Lefebvre E *et al* 2003 Electron and photon production from relativistic laser–plasma interactions *Nucl. Fusion* **43** 629